




Full-polarization angular spectrum modeling of scattered light modulation

RONGJUN SHAO,^{1,†} CHUNXU DING,^{1,†}  YUAN QU,^{1,2}  LINXIAN LIU,³ QIAOZHI HE,² YUEJUN WU,¹
AND JIAMIAO YANG^{1,2,*} 

¹School of Electronic Information and Electrical Engineering, Shanghai Jiao Tong University, Shanghai 200240, China

²Institute of Marine Equipment, Shanghai Jiao Tong University, Shanghai 200240, China

³School of Automation and Software Engineering, Shanxi University, Taiyuan 030006, China

[†]These authors contributed equally to this work.

*Corresponding author: jiamiaoyang@sjtu.edu.cn

Received 25 September 2023; revised 8 January 2024; accepted 8 January 2024; posted 9 January 2024 (Doc. ID 506787);
published 1 March 2024

The exact physical modeling for scattered light modulation is critical in phototherapy, biomedical imaging, and free-space optical communications. In particular, the angular spectrum modeling of scattered light has attracted considerable attention, but the existing angular spectrum models neglect the polarization of photons, degrading their performance. Here, we propose a full-polarization angular spectrum model (*fpASM*) to take the polarization into account. This model involves a combination of the optical field changes and free-space angular spectrum diffraction, and enables an investigation of the influence of polarization-related factors on the performance of scattered light modulation. By establishing the relationship between various model parameters and macroscopic scattering properties, our model can effectively characterize various depolarization conditions. As a demonstration, we apply the model in the time-reversal data transmission and anti-scattering light focusing. Our method allows the analysis of various depolarization scattering events and benefits applications related to scattered light modulation. © 2024 Chinese Laser Press

<https://doi.org/10.1364/PRJ.506787>

1. INTRODUCTION

By modulating the amplitude, phase, or polarization of the optical field, scattered light modulation can compensate the distortion caused by nonuniform microscopic refractive index distributions in a scattering medium, and has been extensively applied in biomedicine, optical communications, and microscopy [1–4]. The practical effectiveness of scattered light modulation is influenced by various factors, such as the scattering dynamics, stochastic properties, and depolarization of the medium [5–8]. To analyze this influence, people often establish a physical model to approximately simulate the scattered light propagation through the medium [9]. An accurate model can provide an effective guidance for optimizing scattered light modulation, thereby improving the focus contrast or the fidelity of the data transmission in the scattering medium.

Currently, several methods have been proposed to simulate the scattering effect, including the transmission matrix [10–13], Monte Carlo and radiative transfer equation [14,15], and angular spectrum [16–18]. The transmission matrix method is commonly used to calculate the change of the optical field before and after propagating through a scattering medium [19]. The Monte Carlo and radiative transfer equation method

is often employed to analyze the energy change of light [20]. Both methods, however, fail to quantify the various factors influencing the modulation effectiveness. In contrast, we have previously developed an angular spectrum model for scattered light modulation [16], which can trace and simulate the propagation of light throughout the system. This model decomposes the complex scattering process into a series of free-space diffraction and random phase shifts so that people can analyze the effects introduced by the medium on the modulation performance. This method has shown a good potential in anti-scattering, high-contrast light focusing, and high-resolution microscopy [21,22]. Furthermore, the angular spectrum model has a good scalability. It can be combined with the optical point-spread function to analyze the degradation of image quality in the scanning microscopy [17]. Combined with the transport theory [18], it can also efficiently analyze the variation of energy during scattering propagation. However, the existing angular spectrum models neglect depolarization occurring in the scattering medium [23,24]. The depolarization can cause a random crosstalk between the two orthogonally polarized channels, affecting the modulation effectiveness. For example, it hinders the high-fidelity data communications in optical fibers [25,26] and restricts the focus contrast generated in biological

tissues [27,28]. Therefore, it is desirable to improve the angular spectrum model to analyze the polarization-related factors for the further development of scattered light modulation.

Here, we establish a full polarization angular spectrum model (*fp*ASM) to describe the scattering of polarized optical fields. As an approximation, we decomposed the field propagation into a series of optical field changes and free-space diffraction. In the model, a Jones matrix simulated the random effects of the scattering particles on the amplitude, phase, and polarization of the optical field; the angular spectrum method simulated the free-space diffraction. We demonstrated the capability of *fp*ASM in time-reversal data transmission and anti-scattering light focusing. We analyzed the influence of different depolarization effects on the modulation effectiveness, including the data fidelity and the focal contrast. Our findings demonstrated that *fp*ASM could properly deal with various depolarization conditions and might benefit further advancements in scattered light modulation.

2. METHODS

Figure 1 illustrates the principle of *fp*ASM. The scattering medium is approximated as a series of scattering planes and nonscattering free spaces. Jones matrices and angular spectrum diffraction are used to calculate the layer-by-layer propagation, tracing the propagation of the scattered optical field. We describe the polarized optical field with a pair of orthogonal bases as

$$\mathbf{E}(x, y) = E_H(x, y)\vec{e}_H + E_V(x, y)\vec{e}_V, \quad (1)$$

where \vec{e}_H and \vec{e}_V represent, respectively, the horizontal and vertical polarization. Either E_H or E_V is the complex amplitude of a polarized component. (x, y) are the Cartesian coordinates. For convenience, we represent the polarized optical field $\mathbf{E}(x, y)$ with a vector $[E_H(x, y); E_V(x, y)]$.

Specifically, we decompose the scattering medium with a thickness of l into M layers of scattering planes arranged at regular intervals [Fig. 1(a)]. Each interval between two adjacent

scattering planes is a free space without a scattering effect. The scattering plane is made up of many pixels [Fig. 1(b)] with a size of D_{pixel} . The scattering caused by a pixel on the optical field can be described in terms of a Jones matrix as

$$\begin{bmatrix} E'_H \\ E'_V \end{bmatrix} = \exp\left(i\frac{\delta}{2}\right) \exp(i\varphi) \times \begin{bmatrix} \cos\frac{\delta}{2} - i\sin\frac{\delta}{2}\cos 2\theta & -i\sin\frac{\delta}{2}\sin 2\theta \\ -i\sin\frac{\delta}{2}\sin 2\theta & \cos\frac{\delta}{2} + i\sin\frac{\delta}{2}\cos 2\theta \end{bmatrix} \begin{bmatrix} E_H \\ E_V \end{bmatrix}, \quad (2)$$

where $[E_H; E_V]$ and $[E'_H; E'_V]$ are the incident and transmitted optical fields, respectively. For convenience, we have omitted the Cartesian coordinates (x, y) in Eq. (2).

Caused by a scattering plane, the common distortion of two fields in orthogonal polarization directions is represented by a complex phase change $\varphi = 2\pi n\Delta l/\lambda + ik$. The refractive index n for an arbitrary pixel in a scattering plane follows the Gaussian distribution with a mean n_{mean} and standard deviation n_{dev} . $\Delta l = l/(M - 1)$ is the distance between the two adjacent scattering planes. k represents the attenuation of amplitude.

The scattering effect on the polarization of light is described by θ and δ . θ represents the angle between the fast axes of the pixels and the x axis, following a uniform distribution of $[-\pi/2, \pi/2]$. δ represents the orthogonal polarization phase difference induced by the fast and slow axes, following the Gaussian distribution with a mean of 0 and a standard deviation of $\delta_{\text{dev}} \in [0, \pi]$. All of these parameters in Eq. (2) make the distortion random, mimicking a scattering medium.

We use the angular spectrum method to calculate the nonscattering free-space diffraction between two adjacent scattering planes [Fig. 1(c)]. We assume that the optical field $[E_{s,H}(x, y); E_{s,V}(x, y)]$ transmitted from the previous scattering plane (source plane) becomes $[E_{d,H}(x, y); E_{d,V}(x, y)]$ in front of the next scattering plane (destination plane). First, a Fourier transformation is calculated for the optical field on the source plane by

$$E_{s,p}(k_x, k_y) = \frac{1}{2\pi} \iint E_{s,p}(x, y) \exp[-i(k_x x + k_y y)] dx dy, \quad (3)$$

where $E_{s,p}$ represents either $E_{s,H}$ or $E_{s,V}$. k_x and k_y correspond to the spatial frequencies in x and y directions, respectively. Upon the propagation from the source plane to the destination plane with a distance Δl , the source optical field $E_{s,p}(k_x, k_y)$ experiences a change and

$$E_{d,p}(k_x, k_y) = E_{s,p}(k_x, k_y) \exp\left[in_0\Delta l \sqrt{\left(\frac{2\pi}{\lambda}\right)^2 - k_x^2 - k_y^2}\right], \quad (4)$$

where n_0 is the refractive index of the free space and λ is the wavelength of light. In the end, the optical field $E_{d,p}(x, y)$ that will interact with the next scattering plane can be obtained as

$$E_{d,p}(x, y) = \frac{1}{2\pi} \iint E_{d,p}(k_x, k_y) \exp[i(k_x x + k_y y)] dk_x dk_y. \quad (5)$$

According to the principle above, by sequentially calculating the Jones matrices of the scattering planes and the diffraction in

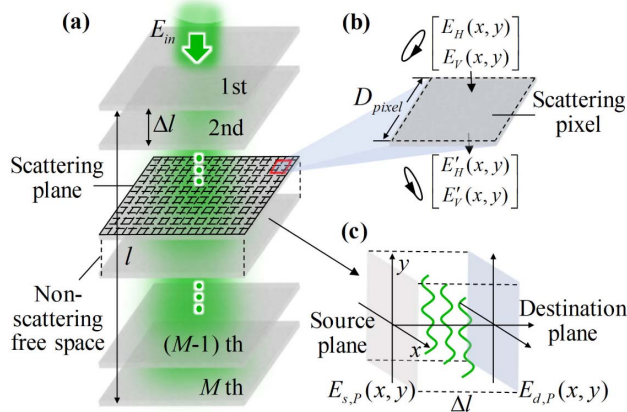


Fig. 1. Principle of *fp*ASM. (a) The scattering medium is approximated as a series of scattering planes and nonscattering free spaces. (b) The scattering plane can be discretized to many pixels with varying optical properties that change the amplitude, phase, and polarization of light. (c) Light propagates in free space from the previous scattering plane (source plane) to the next scattering plane (destination plane).

the free spaces, it becomes possible to effectively describe the scattering propagation of the polarized optical field.

3. MODEL IMPLEMENTATION

To implement the model, all the parameters for the simulation were initialized. We used a collimated laser beam with a wavelength λ of 532 nm and a diameter of 1 mm as the light source. The scattering medium was divided into $M = 81$ scattering planes, with an interval $\Delta l = 20 \mu\text{m}$. The mean and standard deviation of the refractive index were $n_{\text{mean}} = 1.4$ and $n_{\text{dev}} = 1.6 \times 10^{-3}$, respectively [16]. The attenuation factor was $k = 10^{-5}$. The refractive index of the nonscattering free space was $n_0 = 1$. Each plane was discretized into 1000×1000 pixels with a pitch $D_{\text{pixel}} = 5 \mu\text{m}$.

In our model, the macroscopic depolarization property of the scattering medium was determined by the standard deviation δ_{dev} of the orthogonal polarization phase difference in Eq. (2). Therefore, we first established the relationship between this parameter and the mean depolarization distance l_{dp} of the medium. The mean depolarization distance represents the mean distance after which the polarization distribution of the optical field becomes even [29]. Thus, we can calculate l_{dp} by identifying the depth at which the scattered light intensity ratio $I_{s,H}/I_{s,V}$ approximates to 1.

Figure 2(a) shows $I_{s,H}$ and $I_{s,V}$, obtained from the simulation ($\delta_{\text{dev}} = \pi/3$), at the depths of 0.05, 0.30, and 0.60 mm. The intensity ratio $I_{s,H}/I_{s,V}$ approached 1 at the depth of $l_{\text{dp}} = 0.60$ mm. Similarly, we found l_{dp} to be 1.4 mm when $\delta_{\text{dev}} = \pi/5$. We obtained the $I_{s,H}/I_{s,V}$ as a function of depth [Fig. 2(b)]. By measuring $I_{s,H}/I_{s,V}$ and matching the closest points on the curves of different δ_{dev} , the value of δ_{dev} corresponding to an actual medium can be determined. Figure 2(c) shows the relationship between l_{dp} and δ_{dev} . Based on these facts, we could simulate various scattering media by setting different δ_{dev} in our model.

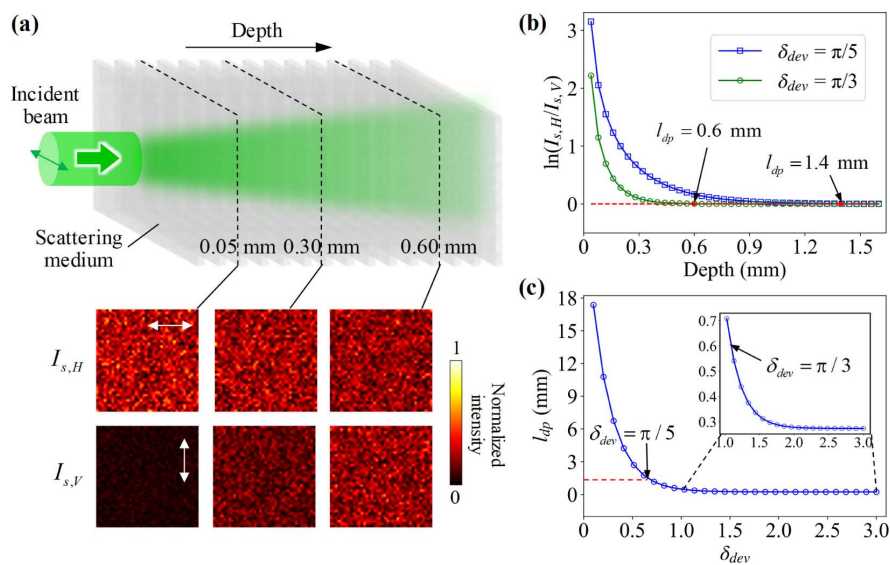


Fig. 2. Characterizing the relationship between the mean depolarization distance and parameter δ_{dev} . (a) Normalized intensity distributions of the scattered light at depths of 0.05 mm, 0.30 mm, and 0.60 mm, respectively. The white arrows indicate the polarization of light. (b) $I_{s,H}/I_{s,V}$ as a function of depth. (c) Mean depolarization distance l_{dp} as a function of the standard deviation δ_{dev} .

4. RESULTS

A. Time-Reversal Data Transmission

A high fidelity of data transmission is crucial for large-channel capacity and long-distance optical communications [30]. In practice, a transmission medium such as multimode fiber often induces polarization crosstalk and reduces the fidelity [19]. Data transmission techniques based on time reversal can compensate the crosstalk [31]. However, the mechanism of how the polarization crosstalk impacts the fidelity remains unclear. For this reason, we simulated the time reversal process with *fp*ASM. In the forward step [Fig. 3(a)], a horizontally polarized image was scrambled by the scattering medium. In the playback step [Fig. 3(b)], the modulated time-reversal optical field propagated backward and recovered the incident image after interacting with the medium.

We calculated the fidelity under various depolarization conditions [Fig. 3(c)]. We used $\ln(I/I_{\text{dp}})$ to characterize different depolarization conditions in the medium. While $\ln(I/I_{\text{dp}})$ was increasing, more and more incident light was depolarized. Our results showed that a full-polarization modulation [27], simultaneously modulating the two orthogonally polarized components propagating backward, could achieve a higher fidelity than a single polarization modulation. Specifically, when the playback component polarized in the same direction as the incident polarization, the fidelity decreased under a strong depolarization due to the polarization crosstalk. Conversely, when playing back in the orthogonal direction, the fidelity exhibited an opposite trend, because the effective information in the vertically polarized component increased with the degree of depolarization. The full-polarization modulation combined the two components so that the polarization crosstalk could be suppressed. Therefore, the full-polarization modulation recovered the image with a higher fidelity than a single polarization modulation in a medium showing a strong depolarization.

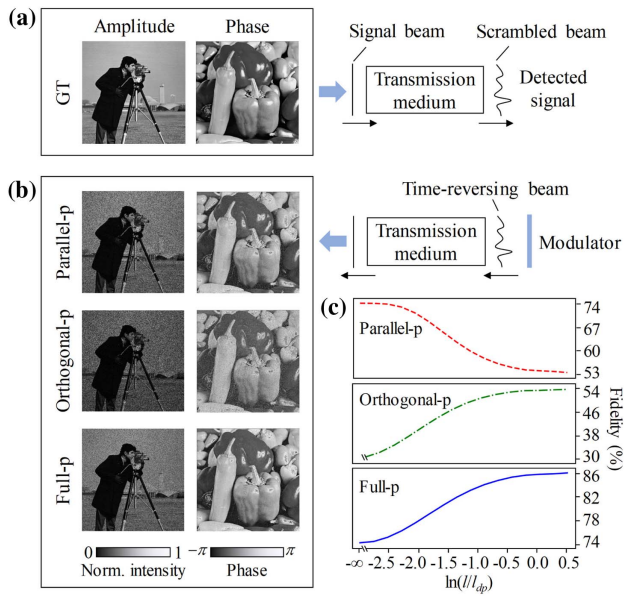


Fig. 3. Time-reversal data transmission. (a) The forward step. The size of the image is 1000×1000 . (b) The playback step. The three results were generated by the parallel polarization modulation (Parallel-p), orthogonal polarization modulation (Orthogonal-p), and full-polarization modulation (Full-p), respectively. We modulated only the phase of optical field. The number of modulation units applied on one polarized component was 10^6 . (c) Fidelity as a function of the degree of depolarization. We used $F = |S_{GT}^* S_{obtained}|^2$ to quantify the fidelity. S_{GT}^* is the conjugate transpose of the incident image and $S_{obtained}$ is the image transmitted through the scattering medium.

B. Anti-Scattering Light Focusing

Scattering depolarization can degrade the contrast of focus [32]. To understand this phenomenon, we first simulated the anti-scattering light focusing with *fp*ASM [Fig. 4(a)]. In this simulation, the lens was modeled by a transmission function $\exp[i\pi(x^2 + y^2)/\lambda f]$ in which $f = 100$ mm. The free-space propagation was calculated by the angular spectrum method. Two holograms I_H and I_V for the two orthogonally polarized components were captured by a camera. From them, we generated two binary patterns $E_{m,H}$ and $E_{m,V}$ for the two digital micromirror devices (DMDs) used in the playback modulation [33]. To focus the light against scattering, the conjugated light modulated by the DMDs propagated backward through a focusing lens. Figure 4(b) shows the simulation results under a strong depolarization condition ($\delta_{dev} = \pi/3$). The three images corresponded to the foci formed by the full, horizontal, and vertical polarization modulation. Represented by the peak-to-background ratio (PBR), the contrast of focus of the full-polarization modulation was larger than that of single polarization modulation by a factor of 2.

In the experimental demonstration, we first quantified the depolarization of a scattering medium [Fig. 4(c)]. Two polarizers were placed before and after the medium. Polarizer 1 set the polarization of incident light from the 532 nm laser (Verdi V5, Coherent, Inc.) and Polarizer 2 selected a particular polarized component in the scattered light. According to the speckles captured by the camera (Basler ace acA1920-155um,

Basler AG), the intensity ratio of the horizontally polarized component to the vertically polarized component was $16.99/17.38 \approx 0.98$, indicating a strong depolarization.

We focused light against this scattering medium. The number of controlled optical modes of one DMD (JUOPT-DLP 7000, JUOPT Technology Co., Ltd.) was $48 \times 48 = 2304$. The peak intensity and PBR of focus of full-polarization modulation were higher than those of the other two methods by factors of four and two, respectively [Fig. 4(d)]. Furthermore, we analyzed the contrast of focus under various depolarization conditions [Fig. 4(e)]. The PBR of the full-polarization modulation was not affected by the change of depolarization conditions and kept at a high level. In comparison, the PBRs were declining considerably while the degree of depolarization was increasing if we modulated only the horizontally or vertically polarized component because half of the information carried by the light was lost without an effective control. The result demonstrated that *fp*ASM could help to improve the contrast of anti-scattering light focusing.

5. DISCUSSION AND CONCLUSION

We have proposed *fp*ASM, an optimized angular spectrum method modeling the polarized light propagation for scattered light modulation. This model decomposes the scattering medium into a series of scattering planes and free spaces, with the Jones matrices describing the distortion on amplitude, phase, and polarization of the scattered light and the angular spectrum method calculating the free-space propagation. We established the relationship between several model parameters and the macroscopic properties of the scattering medium. With this model, we first analyzed the influence of depolarization on the fidelity of time-reversal data transmission, and found that the full-polarization modulation provided the best fidelity among the three modulation methods. Then, we analyzed the influence of depolarization on the contrast of anti-scattering light focusing and found that the contrast of focus generated by the full polarization modulation was higher than that of single polarization modulation by a factor of 2, under the strong depolarization condition.

We introduced the Jones matrix to simulate the scattering distortion on the information of the light field, which made each pixel in the scattering plane appear to be a birefringent crystal in form. Nevertheless, this did not limit the applicability of our model to different scattering media. Instead, we just applied the clothing of the familiar optical process to approximately simulate the unknown scattering propagation inside the medium. By setting some random parameters, which were not even clearly defined in the actual scattering media but could be determined according to the scattering phenomenon of media, we made the multi degrees-of-freedom information change process no longer birefringent but an approximation of a random scattering event. As the results showed, lots of repetitions of random birefringent events and free-space diffraction could indeed effectively complete the simulation of multiple scattering.

Besides the scattered light modulation based on time reversal, other methods can benefit from *fp*ASM. For example, by incorporating fast decorrelation components [16], our model

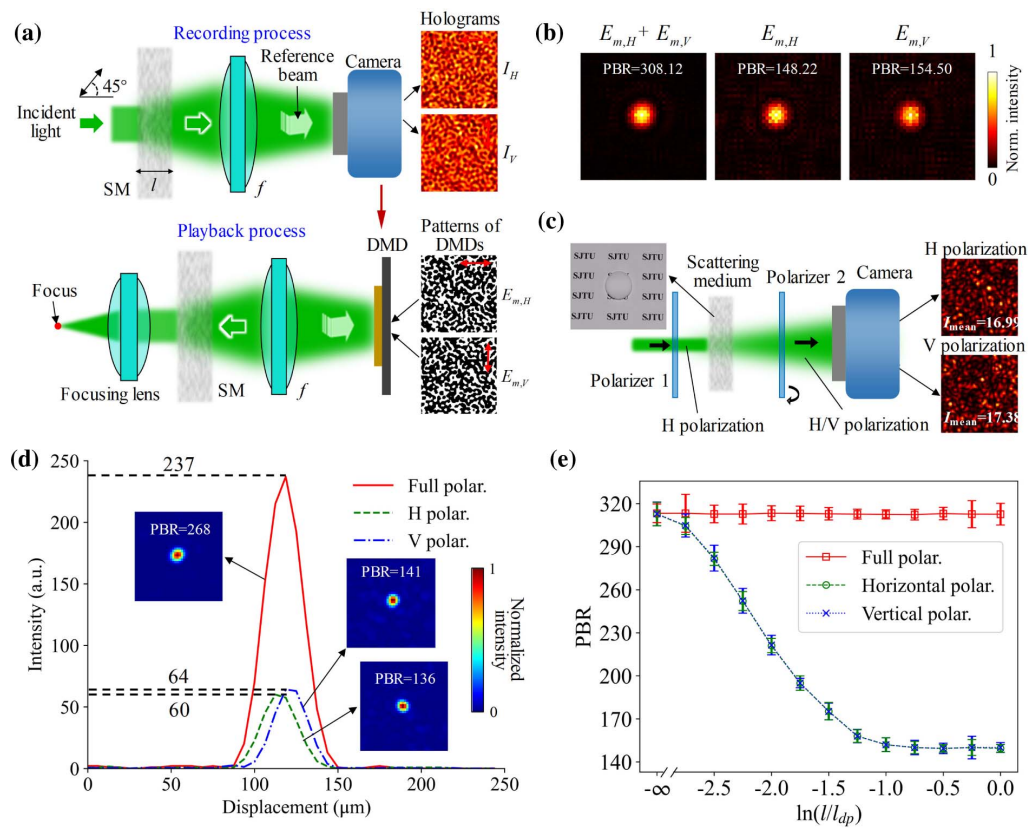


Fig. 4. Anti-scattering light focusing. (a) Procedure of anti-scattering light focus. First, record the holograms of the scattered optical fields. Second, play back the conjugate optical fields. (b) Simulation of three different modulation methods. (c) Verification of depolarization property of the scattering medium (#34–473, Edmund Optics, Inc.). (d) Profiles of foci generated by the three different modulation methods. (e) PBR as a function of the degree of depolarization.

has the potential to evaluate whether the speed of the feedback-based optimization methods [5] meets the dynamic scattering. Moreover, the fp ASM can be further improved. First, we assumed that the incident light was highly coherent. Therefore, a comprehensive model for the incoherent light, based on the incoherent diffraction transmission theory [34], is warranted. Second, fp ASM considered only the forward propagation of the optical field in the scattering medium and neglected reflection. Adding a weak reflection layer may produce a more accurate model [18]. Third, introducing a controllable guide star can enable focusing within a scattering medium and analyze its internal dynamics [16,35].

In addition, many applications may benefit from our model. For example, by focusing light against scattering in a tissue, a photo-therapist can optimize the dosage, minimizing the damage to normal cells [36]; by analyzing the detrimental effects of scattering on the image quality, the resolution of optical microscopy may be further improved [37]; the scattering effect of liquid crystal polarization optical elements may be simulated to support high-resolution augmented reality and virtual reality [38]; and, after quantifying the dynamics of atmosphere, our model also has the potential to mitigate the negative impacts of turbulence in free-space optical communications [39]. Therefore, we expect this approach to support advancements in biomedicine, imaging, and optical communications in the future.

Funding. National Natural Science Foundation of China (62205189, 62375171); Fundamental Research Funds for the Central Universities; Shanghai Pujiang Program (22PJ1407500); Shanghai Jiao Tong University 2030 Initiative (WH510363001-10); Oceanic Interdisciplinary Program of Shanghai Jiao Tong University (SL2022ZD205); Science Foundation of Donghai Laboratory (DH-2022KF01001).

Disclosures. The authors have no conflicts of interest to disclose.

Data Availability. Data underlying the results presented in this paper are not publicly available at this time but may be obtained from the authors upon reasonable request.

REFERENCES

1. I. Remer, R. Shaashoua, N. Shemesh, *et al.*, "High-sensitivity and high-specificity biomechanical imaging by stimulated Brillouin scattering microscopy," *Nat. Methods* **17**, 913–916 (2020).
2. Y. Luo, S. Yan, H. Li, *et al.*, "Towards smart optical focusing: deep learning-empowered dynamic wavefront shaping through nonstationary scattering media," *Photon. Res.* **9**, B262–B278 (2021).
3. H. Li, Z. Yu, T. Zhong, *et al.*, "Towards ideal focusing of diffused light via optical wavefront shaping," *Adv. Photon.* **5**, 020502 (2023).

4. Y. Liu, Z. Zhang, P. Yu, *et al.*, "Learning-enabled recovering scattered data from twisted light transmitted through a long standard multimode fiber," *Appl. Phys. Lett.* **120**, 131101 (2022).
5. J. Yang, Q. He, L. Liu, *et al.*, "Anti-scattering light focusing by fast wavefront shaping based on multipixel encoded digital-micromirror device," *Light Sci. Appl.* **10**, 149 (2021).
6. P. Yu, Y. Liu, Y. Wu, *et al.*, "Dynamic polarization holographic projection enabled by a scattering material-based reconfigurable hologram," *ACS Photon.* **9**, 3712–3719 (2022).
7. Q. Zhao, S. Tu, Q. Lei, *et al.*, "Creation of cylindrical vector beams through highly anisotropic scattering media with a single scalar vector transmission matrix calibration," *Photon. Res.* **10**, 1617–1623 (2022).
8. Y. Luo, Y. Zhao, J. Li, *et al.*, "Computational imaging without a computer: seeing through random diffusers at the speed of light," *eLight* **2**, 4 (2022).
9. Z. Yu, H. Li, T. Zhong, *et al.*, "Wavefront shaping: a versatile tool to conquer multiple scattering in multidisciplinary fields," *Innovation* **3**, 623–637 (2022).
10. S. M. Popoff, G. Leroose, R. Carminati, *et al.*, "Measuring the vector transmission matrix in optics: an approach to the study and control of light propagation in disordered media," *Phys. Rev. Lett.* **104**, 100601 (2010).
11. A. Boniface, M. Mounaix, B. Blochet, *et al.*, "Transmission-matrix-based point-spread-function engineering through a complex medium," *Optica* **4**, 54–59 (2017).
12. S. Li, C. Saunders, D. J. Lum, *et al.*, "Compressively sampling the optical vector transmission matrix of a multimode fibre," *Light Sci. Appl.* **10**, 88 (2021).
13. A. d'Arco, F. Xia, A. Boniface, *et al.*, "Physics-based neural network for non-invasive control of coherent light in scattering media," *Opt. Express* **30**, 30845–30856 (2022).
14. L. Wang, S. L. Jacques, and L. Zheng, "MCML—Monte Carlo modeling of light transport in multi-layered tissues," *Comput. Methods Programs Biomed.* **47**, 131–146 (1995).
15. W. Cai, M. Lax, and R. Alfano, "Cumulant solution of the elastic Boltzmann transport equation in an infinite uniform medium," *Phys. Rev. E* **61**, 3871–3876 (2000).
16. J. Yang, J. Li, S. He, *et al.*, "Angular-spectrum modeling of focusing light inside scattering media by optical phase conjugation," *Optica* **6**, 250–256 (2019).
17. X. Cheng, Y. Li, J. Mertz, *et al.*, "Development of a beam propagation method to simulate the point spread function degradation in scattering media," *Opt. Lett.* **44**, 4989–4992 (2019).
18. M. Yan, M. Gong, and J. Ma, "Extended angular-spectrum modeling (EASM) of light energy transport in scattering media," *Opt. Express* **31**, 2860–2876 (2023).
19. L. Gong, Q. Zhao, H. Zhang, *et al.*, "Optical orbital-angular-momentum-multiplexed data transmission under high scattering," *Light Sci. Appl.* **8**, 27 (2019).
20. A. Krasnoshchoka, A. K. Hansen, A. Thorseth, *et al.*, "Phosphor material dependent spot size limitations in laser lighting," *Opt. Express* **28**, 5758–5767 (2020).
21. Z. Cheng and L. V. Wang, "Focusing light into scattering media with ultrasound-induced field perturbation," *Light Sci. Appl.* **10**, 159 (2021).
22. A. Thendiyammal, G. Osnabrugge, T. Knop, *et al.*, "Model-based wavefront shaping microscopy," *Opt. Lett.* **45**, 5101–5104 (2020).
23. H. B. de Aguiar, S. Gigan, and S. Brasselet, "Polarization recovery through scattering media," *Sci. Adv.* **3**, e1600743 (2017).
24. J. Yang, Y. Shen, Y. Liu, *et al.*, "Focusing light through scattering media by polarization modulation based generalized digital optical phase conjugation," *Appl. Phys. Lett.* **111**, 201108 (2017).
25. M. Mounaix and J. Carpenter, "Control of the temporal and polarization response of a multimode fiber," *Nat. Commun.* **10**, 5085 (2019).
26. W. Xiong, C. W. Hsu, Y. Bromberg, *et al.*, "Complete polarization control in multimode fibers with polarization and mode coupling," *Light Sci. Appl.* **7**, 54 (2018).
27. Y. Shen, Y. Liu, C. Ma, *et al.*, "Focusing light through scattering media by full-polarization digital optical phase conjugation," *Opt. Lett.* **41**, 1130–1133 (2016).
28. L. Liu, C. Ding, Y. Qu, *et al.*, "Anti-scattering light focusing by full-polarization wavefront shaping based on digital micromirror devices," *Appl. Phys. Express* **15**, 092001 (2022).
29. D. A. Zimnyakov, V. V. Tuchin, and A. G. Yodh, "Characteristic scales of optical field depolarization and decorrelation for multiple scattering media and tissues," *J. Biomed. Opt.* **4**, 157–163 (1999).
30. Q. Zhang, S. Rothe, N. Koukourakis, *et al.*, "Learning the matrix of few-mode fibers for high-fidelity spatial mode transmission," *APL Photon.* **7**, 066104 (2022).
31. Y. Zhou, B. Braverman, A. Fyffe, *et al.*, "High-fidelity spatial mode transmission through a 1-km-long multimode fiber via vectorial time reversal," *Nat. Commun.* **12**, 1866 (2021).
32. Z. Cheng, J. Yang, and L. V. Wang, "Dual-polarization analog optical phase conjugation for focusing light through scattering media," *Appl. Phys. Lett.* **114**, 231104 (2019).
33. L. Liu, W. Liang, Y. Qu, *et al.*, "Anti-scattering light focusing with full-polarization digital optical phase conjugation based on digital micromirror devices," *Opt. Express* **30**, 31614–31622 (2022).
34. Z. Zhong and S. Zhao, "Modified angular spectrum algorithm for the propagation of partially coherent beams in optical systems," *J. Opt. Soc. Am. A* **40**, 741–746 (2023).
35. A. Khadria, C. D. Paavola, Y. Zhang, *et al.*, "Long-duration and non-invasive photoacoustic imaging of multiple anatomical structures in a live mouse using a single contrast agent," *Adv. Sci.* **9**, 2202907 (2022).
36. H. Shi and P. J. Sadler, "How promising is phototherapy for cancer?" *Br. J. Cancer* **123**, 871–873 (2020).
37. N. G. Horton, K. Wang, D. Kobat, *et al.*, "In vivo three-photon microscopy of subcortical structures within an intact mouse brain," *Nat. Photonics* **7**, 205–209 (2013).
38. J. Xiong and S. T. Wu, "Planar liquid crystal polarization optics for augmented reality and virtual reality: from fundamentals to applications," *eLight* **1**, 3 (2021).
39. M. P. J. Lavery, C. Peuntinger, K. Gunthner, *et al.*, "Free-space propagation of high-dimensional structured optical fields in an urban environment," *Sci. Adv.* **3**, e1700552 (2017).